Solar Phys (2007) 240: 373–386
DOI 10.1007/s11207-006-0101-x

The Dependence of the Geoeffectiveness of Interplanetary Flux Rope on Its Orientation, with Possible Application to Geomagnetic Storm Prediction

Yuming Wang · Pinzhong Ye · S. Wang

Received: 2 November 2005 / Accepted: 23 November 2006 /
Published online: 28 February 2007

Abstract Interplanetary magnetic clouds (MCs) are one of the main sources of large non-recurrent geomagnetic storms. With the aid of a force-free flux rope model, the dependence of the intensity of geomagnetic activity (indicated by *Dst* index) on the axial orientation (denoted by θ and ϕ in GSE coordinates) of the magnetic cloud is analyzed theoretically. The distribution of the *Dst* values in the (θ, ϕ) plane is calculated by changing the axial orientation for various cases. It is concluded that (i) geomagnetic storms tend to occur in the region of $\theta < 0°$, especially in the region of $\theta \lesssim -45°$, where larger geomagnetic activity could be created; (ii) the intensity of geomagnetic activity varies more strongly with θ than with ϕ; (iii) when the parameters B_0 (the magnetic field strength at the flux rope axis), R_0 (the radius of the flux rope), or V (the bulk speed) increase, or $|D|$ (the shortest distance between the flux rope axis and the x-axis in GSE coordinates) decreases, a flux rope not only can increase the intensity of geomagnetic activity, but also is more likely to create a storm, however the variation of n (the density) only has a little effect on the intensity; (iv) the most efficient orientation (MEO) in which a flux rope can cause the largest geomagnetic activity appears at $\phi \sim 0°$ or $\sim 180°$, and some value of θ which depends mainly on D; (v) the minimum *Dst* value that could be caused by a flux rope is the most sensitive to changes in B_0 and V of the flux rope, and for a stronger and/or faster MC, a wider range of orientations will be geoeffective. Further, through analyzing 20 MC-caused moderate to large geomagnetic storms during 1998 – 2003, a long-term prediction of MC-caused geomagnetic storms on the basis of the flux rope model is proposed and assessed. The comparison between the theoretical results and the observations shows that there is a close linear correlation between the estimated and observed minimum *Dst* values. This suggests that using the ideal flux rope to predict practical MC-caused geomagnetic storms is applicable. The possibility of the long-term prediction of MC-caused geomagnetic storms is discussed briefly.

Keywords Magnetic clouds · Geomagnetic storms · Flux rope · Prediction

Y. Wang (✉) · P. Ye · S. Wang
CAS Key Laboratory of Basic Plasma Physics, School of Earth & Space Sciences,
University of Science & Technology of China, Hefei, Anhui 230026, People's Republic of China
e-mail: ymwang@ustc.edu.cn

1. Introduction

Geomagnetic activity, often quantified by the *Dst* indicator, is one of the most important influences on the environment around the Earth. Traditionally, significant geomagnetic activity (*Dst* index ≤ -30 nT) is called a geomagnetic storm. Large non-recurrent geomagnetic storms are usually caused by interplanetary ejecta (especially magnetic clouds, MCs) and shock sheaths (or compressed solar wind plasma) preceding them (*e.g.*, Sheeley *et al.*, 1985; Gosling *et al.*, 1991; Gonzalez *et al.*, 1994). These interplanetary disturbances create geomagnetic storms through changing some parameters of the interplanetary medium.

The relationship between interplanetary parameters and the intensity of geomagnetic activity has been studied exhaustively in the past several decades (*e.g.*, Burton, McPherron, and Russell, 1975; Perreault and Akasofu, 1978; Gonzalez and Tsurutani, 1987; Gonzalez *et al.*, 1989; Tsurutani and Gonzalez, 1995; Wang *et al.*, 2003b). Many empirical formulae have been developed to estimate *Dst* index as a function of interplanetary parameters observed at 1 AU (*e.g.*, Burton, McPherron, and Russell, 1975; Perreault and Akasofu, 1978; Vasyliunas *et al.*, 1982; Murayama, 1986; Fenrich and Luhmann, 1998; O'Brien and McPherron, 2000; Lundstedt, Gleisner, and Wintoft, 2002; Temerin and Li, 2002; Wang, Chao, and Lin, 2003a; Wang *et al.*, 2003b). It is well known that a fast solar wind speed (V), a strong southward component (B_s) of the interplanetary magnetic field (IMF), and a long duration (Δt) of southward IMF, are the most important factors contributing to large geomagnetic storms (*e.g.*, Gonzalez *et al.*, 1994).

As one of the main drivers of geomagnetic storms, MCs are usually treated as loop-like flux ropes, and may be modeled by a force-free flux rope (*e.g.*, Burlaga, 1988; Lepping, Jones, and Burlaga, 1990; Kumar and Rust, 1996), which is given by the Lundquist (1950) solution in local cylindrical coordinates (R, Φ, Z): $B_R = 0$, $B_\Phi = H B_0 J_1(\alpha R)$, $B_Z = B_0 J_0(\alpha R)$, where $H = \pm 1$ indicates the handedness, B_0 is the magnetic field strength at the axis of the flux rope, and J_0 and J_1 are Bessel functions of order 0 and 1, respectively. The model describes a short, straight flux rope, which approximately represents a relatively short segment of the gigantic, curved flux rope with feet on the Sun, that is usually suggested to produce the MC signature. Figure 1 shows the sketch of a flux rope. The orientation of the flux rope's axis (*i.e.*, the orientation of axial magnetic field, also called MC orientation for short) can be denoted by θ and ϕ, *i.e.*, the elevation and azimuthal angles in GSE coordinates. $\theta = 0°$ corresponds to the axial magnetic field parallel to the ecliptic plane, and $\theta = 90°$ refers to the axial magnetic field pointing to ecliptic north. Similarly $\phi = 0°$ or $180°$ correspond to the axial magnetic field toward or away from the Sun, and $\phi = 90°$ and $270°$, the axial magnetic field pointing to east and west, respectively. It is obvious that, for an identical MC, the intensity of the associated geomagnetic activity will vary with changing its orientation because B_s and Δt, the two interplanetary causes of geomagnetic activity, are closely dependent on the MC orientation. Hence, the MC orientation is an important factor in affecting the intensity of geomagnetic activity (Zhao, 2002).

The force-free flux rope model is one in which the strongest magnetic field is at and along the axis of the flux rope. However, it does not mean that a flux rope with orientation at $\theta = -90$, *i.e.*, completely southward, reaches its largest geoeffectiveness. The orientation (called the most efficient orientation, MEO) associated with the largest geoeffectiveness should be at the best combination of B_s and Δt. Besides, the MEO depends on many other MC parameters, such as the magnetic field strength, solar wind speed, the distance of the Earth from the flux rope axis, etc. This paper will present a clear theoretical picture of the flux rope's geoeffectiveness depending on its orientation, and determine in which orientation a flux rope-like MC is the most geoeffective. Then by analyzing 20 MC-caused geomagnetic

storms, a comparison between the theoretical results and observations is made to illustrate the value and applicability of using an ideal flux rope model to predict real MC-caused geomagnetic activity. Strictly, a storm should be evaluated by two parameters, the storm duration and the minimum *Dst* value. This study will only consider the minimum *Dst* value.

2. Theoretical Results of Flux Rope's Geoeffectiveness Depending on Its Orientation

2.1. *Dst* Estimation by Flux Rope Model

The Wang, Chao, and Lin (2003a) model for predicting the *Dst* index based on solar wind data at 1 AU is an improvement over the O'Brien and McPherron (2000) model. The Wang, Chao, and Lin (2003a) model is described as below

$$\begin{cases} \mathrm{d}Dst^*/\mathrm{d}t = Q - Dst^*/\tau, \\ Dst^* = Dst - 7.26\sqrt{P} + 11 \text{ nT}, \\ Q = \begin{cases} 0, & VB_s \le 0.49 \text{ mV/m}, \\ -4.4(VB_s - 0.49)(P/P_0)^{\gamma}, & VB_s > 0.49 \text{ mV/m}, \end{cases} \\ \tau = \begin{cases} 8.70\mathrm{e}^{6.66/(6.04+P)}, & B_z \ge 0, \\ 2.40\mathrm{e}^{9.74/(4.69+VB_s)}, & B_z < 0, \end{cases} \end{cases} \tag{1}$$

where V is the solar wind speed, B_s is the southward component of the IMF ($B_s = 0$ when $B_z \ge 0$ and $B_s = -B_z$ when $B_z < 0$), $P = mnV^2$ is the solar wind dynamic pressure, and τ is the decay time. The power index γ and constant P_0 are 0.2 and 3.0 nPa, respectively.

In order to calculate the predicted geomagnetic activity intensity, Dst_p, during any interval of interest, $B_z(t)$, $V(t)$ and density $n(t)$ must be specified. Usually these variables can be acquired from the observations of, for example, the ACE and Wind spacecraft. Here, for a theoretical analysis of flux rope's geoeffectiveness, $B_z(t)$ will be derived from the parameters that determine the magnetic configuration and the position of the flux rope in GSE coordinates (seen in Figure 1). These parameters include B_0, $H = \pm 1$, R_0 (the flux rope radius), θ, ϕ, and D (the signed shortest distance between the flux rope axis and the GSE x-axis, indicating how close the flux rope axis gets as it passes by the Earth or any spacecraft at the L1 libration point such as ACE). It should be noticed that for any given θ and ϕ, except $\theta = 0°$ and $\phi = 0°$ or 180°, there are two possible flux rope axes for a certain shortest distance ($|D|$), and the directions from the GSE x-axis to the two axes along the lines measuring the shortest distance are in the $y-z$ plane and anti-parallel which are distinguished by the sign of D. $D > 0$ and < 0 means that the direction is in the range of (−90°, 90°] and (90°, 270°] anticlockwise from z-axis in the $y-z$ plane, respectively, *i.e.*, the flux rope axis is above/below the GSE x-axis, and $D = 0$ means flux rope axis just crosses the GSE x-axis. Moreover, we will not consider the case that $\theta = 0°$ and $\phi = 0°$ or 180°, because at the two orientations, the flux rope axis is completely parallel to the GSE x-axis and, in theory, the duration of the Earth staying in the flux rope would be infinite. For simplicity, the other two variables $V(t)$ and $n(t)$ are both assumed to be constant inside the flux rope.

2.2. Results

By using the above method, the effect of MC orientation on the intensity of geomagnetic activity is studied. For a flux rope with $B_0 = 20$ nT, $H = -1$, $R_0 = 0.15$ AU, $D = 0.0R$,

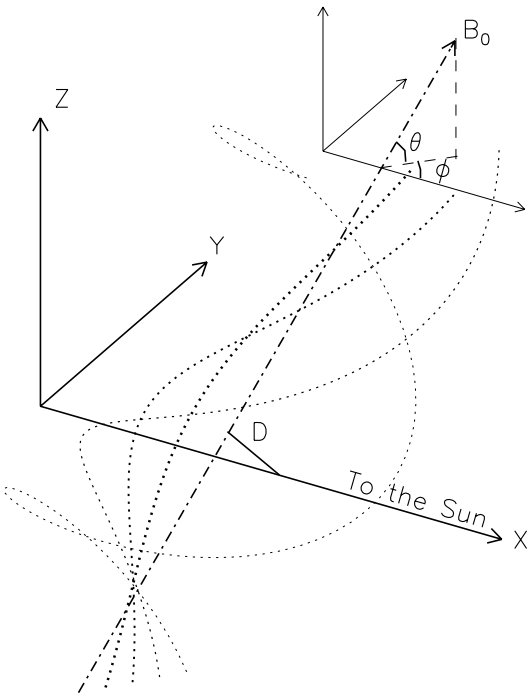

Figure 1 Sketch of a force-free flux rope in GSE coordinates. Dotted lines show the helical magnetic field lines. Flux rope orientation is the direction of **B** at the axis as indicated by the dash-dotted arrow. $|D|$ denotes the shortest distance between the flux rope axis and the GSE x-axis.

$V = 500$ km s^{-1}, and $n = 10$ cm^{-3}, the estimated Dst_p as a function of the MC orientation is shown in the left panel of Figure 2a. The dashed curve denotes the level of -30 nT, at which a geomagnetic storm can be defined, and therefore we name the region below this level the 'storm region' (SR). The solid curve denotes the level of $0.9Dst_{pmin}$, and we call the region with $Dst_p \leq 0.9Dst_{pmin}$ as the 'efficient region' (ER) because within the region the flux rope almost reaches its strongest geoeffectiveness. It is found that in this case the Dst_p distribution is almost symmetrical with respect to $\phi = 0°$ and 180° in the (θ, ϕ) plane. Geomagnetic storms mainly appear at negative θ, especially in the ER of $-90° < \theta \leq\sim -70°$. The surface plot represented in the right panel shows clearly that intensity varies significantly with changing orientation, and this variation is more sensitive to θ than to ϕ.

Figures 2b and 2c exhibit two other cases in which the GSE x-axis and the axis of the flux rope are not crossed, but $0.2R_0$ away from each other, *i.e.*, $D = \pm 0.2R_0$. It should be mentioned that, when $\theta \neq \pm 90°$, $D \neq 0$, and ϕ crosses 0° or 180°, D will change its sign. That is to say, if D was $-0.2R_0$ in $0° \leq \phi < 180°$, D would be $0.2R_0$ in $180° \leq \phi < 360°$, and *vice versa*. Thus there are two Dst_p distributions (b) and (c) for the case of $D = \pm 0.2R_0$. Compared with distribution (a), these two distributions are still approximately symmetrical about $\phi = 0°$ and 180°, and their SRs and ERs are also in the negative θ region, but their shapes have changed significantly. On the other hand, the only difference between distributions (b) and (c) is that the two parts in $0° \leq \phi < 180°$ and $180° \leq \phi < 360°$ are exchanged. The symmetries appearing in distributions (b) and (c) suggest that the sign of D does not affect the Dst_p distribution fundamentally. In addition, we find that changing the handedness H of the flux rope is the same as changing the sign of D, *i.e.*, if $H = -1$ in case (b) was changed to $H = 1$, the Dst_p distribution would be distribution (c). Thus the sign of the helicity of flux ropes also does not affect the Dst_p distribution fundamentally. So hereafter, we only consider the distribution in the region $0° \leq \phi < 180°$ with $H = -1$ and $D \geq 0$.

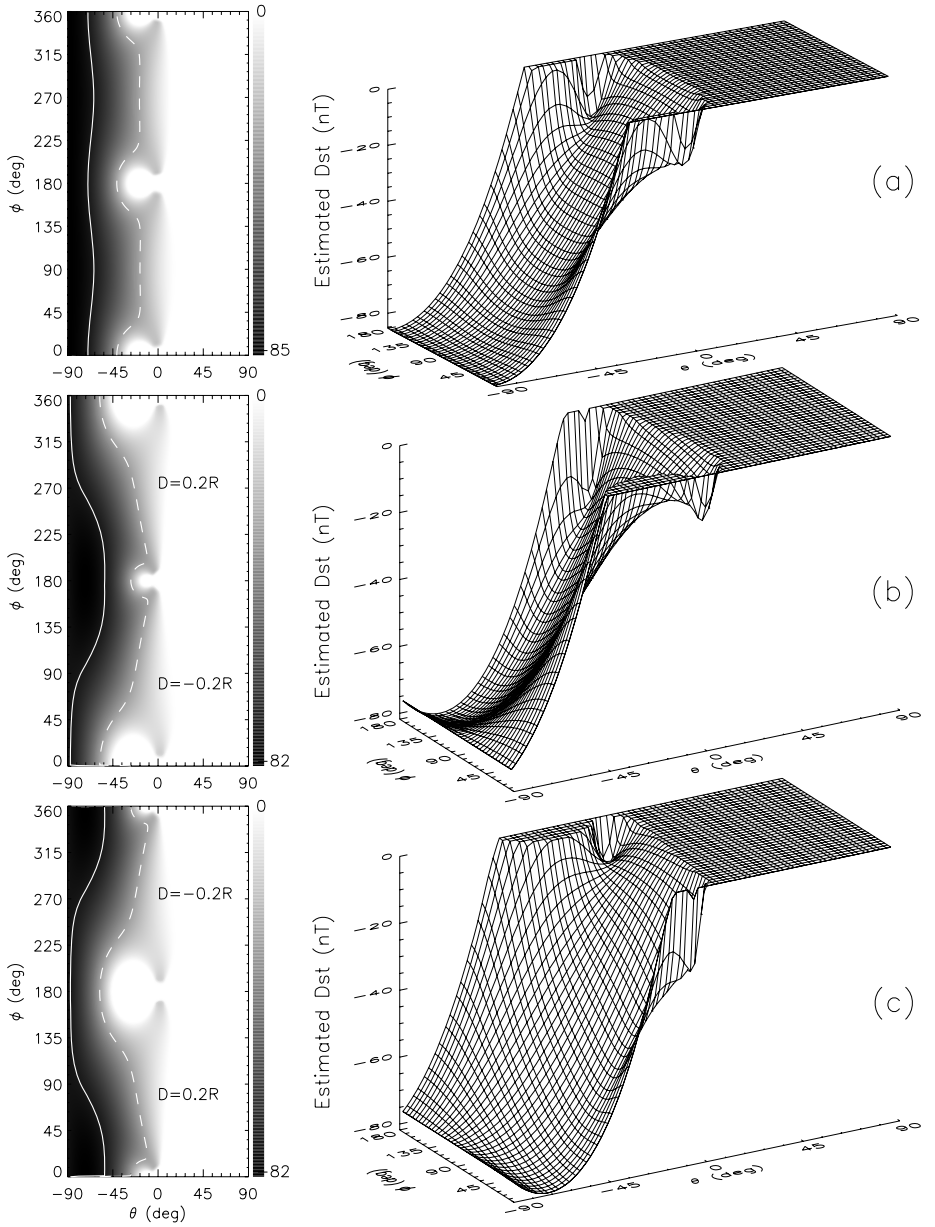

Figure 2 (a) The estimated Dst_p as a function of the elevation θ and azimuthal ϕ of the axis of the flux rope, for the case where $B_0 = 20$ nT, $H = -1$, $R_0 = 0.15$ AU, $D = 0.0R_0$, $V = 500$ km s^{-1}, and $n = 10$ cm^{-3}. The left panel presents the gray-scale contour of Dst_p in the (θ, ϕ) plane. The right panel shows a 3D view, in which only the region $0° < \phi < 180°$ is presented. (b) and (c): Two cases in which all the parameters are the same as in those case (a) except that $D = \pm 0.2R_0$. The dashed and solid lines denote the SRs and ERs, respectively.

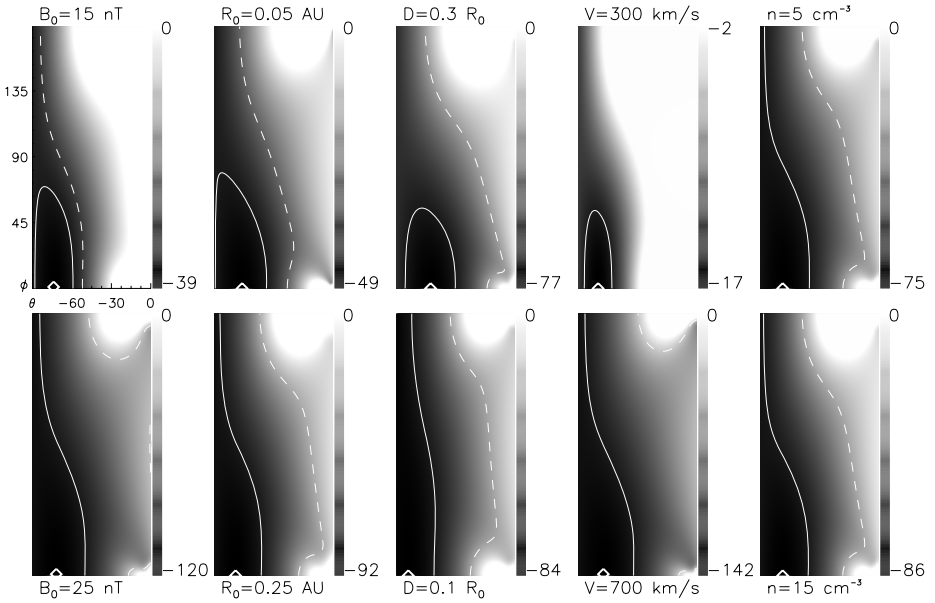

Figure 3 Dst_p distributions for different values of, from the most left column to the most right column, B_0, R_0, D, V and n, respectively. The gray scale is in the units of nT as indicated in the right side of each sub-figure. In each case, the start point is the situation of Figure 2c, and only one parameter has been varied. The SRs and ERs are denoted by the dashed and solid curves, respectively. The diamonds denote the most efficient orientation (MEO) of the flux rope to cause the largest geomagnetic disturbance.

Figure 3 shows more cases. The columns from the left to right represent the different Dst_p distributions obtained by changing B_0, R_0, D, V, and n, respectively. In each case, the start point is the situation of Figure 2c, and only one parameter has been varied. Because Dst_p distributions are symmetrical about $\phi = 180°$ and storms preferentially appear at negative θ, only the region of $0° \leq \phi < 180°$ (scaled on the y-axis) and $-90° \leq \theta < 0°$ (scaled on the x-axis) is plotted. As shown in these plots, the minimum value of Dst_p becomes more negative as B_0, R_0, V or n increases or $|D|$ decreases, and the SR and ER indicated by the dashed and solid curves enlarge with the same changes of the above parameters except for n. The ER always appears in the region of $\theta \lesssim -45°$. The last column of Figure 3 reveals that the shape of the Dst_p distribution is almost independent of n.

The decreased minimum value of Dst_p and enlarged SR and ER suggest that, with larger B_0, R_0 and/or V, and/or smaller $|D|$, a flux rope not only can increase the geomagnetic activity intensity (for the more negative minimum of Dst_p), but also is more likely to create a storm (for the larger area of SR and ER). These results are reasonable because larger B_0 and/or V can produce larger VB_s, larger R_0 can not only give a longer duration of B_s but also indeed increase the total magnetic flux of B_s passing the Earth due to the larger cross-sectional area of the flux rope, and smaller distance from the flux rope axis leads to both a longer duration of B_s and a stronger magnetic field along the axial direction in terms of the pitch angle of the helix (Figure 1).

Further, the variation of the most efficient orientation (MEO), in which a flux rope can cause the largest geomagnetic activity, is analyzed. The diamonds in Figure 3 have marked the MEOs of those cases. The variation of MEO is displayed more clearly in the upper panel of Figure 4, in which all the parameters, B_0, R_0, D, V and n, vary in their own

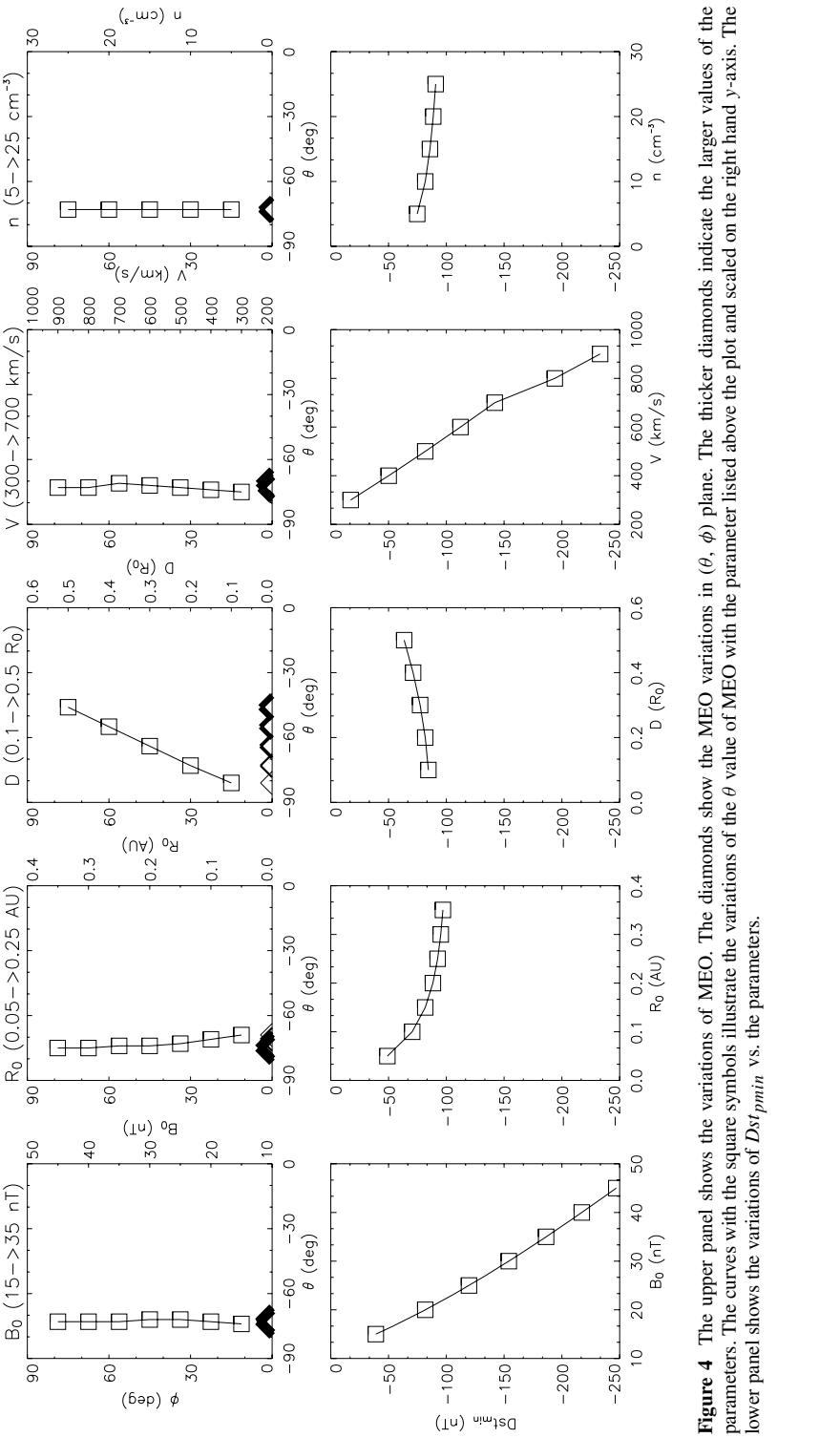

Figure 4 The upper panel shows the variations of MEO. The diamonds show the MEO variations in (θ, ϕ) plane. The thicker diamonds indicate the larger values of the parameters. The curves with the square symbols illustrate the variations of the θ value of MEO with the parameter listed above the plot and scaled on the right hand y-axis. The lower panel shows the variations of Dst_{pmin} vs. the parameters.

reasonable range. It is found that, in all the cases, the MEO appears at $\phi \sim 0°$ (or $\sim 180°$ due to the symmetries of the distributions as shown in Figure 2) and a certain value of θ that depends on variable parameters. Particularly, the θ value of MEO evidently varies with D. For example, θ is $\sim -73°$ for a flux rope with $B_0 = 20$ nT, $H = -1$, $R_0 = 0.15$ AU, $|D| = 0.2R_0$, $V = 500$ km s^{-1} and $n = 10$ cm^{-3} (*i.e.*, the cases exhibited in Figure 2b and 2c), but θ decreases to $-90°$ when the GSE x-axis crosses the axis of the flux rope, *i.e.*, $D = 0$. This is reasonable due to the helical magnetic field inside the flux rope (Figure 1). The magnetic field direction will deviate from perpendicular to parallel to the axis of the flux rope as one approaches it, and importantly, the magnetic field strength will increase meanwhile. The variation of MEO with B_0, R_0 and V is relatively insignificant, and the MEO is independent of n as the shape of the Dst_p distribution is independent.

In addition, the lower panel of Figure 4 illustrates how large a geomagnetic storm could be caused by a flux rope with various parameters. It is found that the Dst_{pmin} is the most sensitive to changes in B_0 and V. In our cases, when B_0 increases from 15 to 35 nT or V increases from 300 to 700 km s^{-1}, the value of Dst_{pmin} decreases linearly from minus tens nT to less than -200 nT. For other three parameters, Dst_{pmin} does not change so much. The minimum value of Dst appears at $\mathrm{d}Dst/\mathrm{d}t = 0$. So $Dst_{pmin} \sim \tau Q$, according to (1), and that implies that Dst_{pmin} is approximately proportional to B_0 and V. Thus, the linear change of Dst value with the change of B_0 and V could be expected. Similarly, Dst_{pmin} is approximately proportional to n^{γ}, and therefore the curve for n is very flat as shown in the figure. It is not so straightforward for R_0 and D, but more negative values of Dst with increasing R_0 and decreasing D are expected, as both imply stronger magnetic fields at the observation point. This result is consistent with previous empirical studies of the relationship between the interplanetary parameters and geomagnetic storm intensity, in which the solar wind speed and the southward magnetic field strength are the most important (*e.g.*, Gonzalez *et al.*, 1994). One should notice that the more negative Dst_{pmin} means the larger sensitivity of the intensity of geomagnetic activity to the MC orientation. Thus, for a stronger, faster, larger, and/or denser magnetic cloud, its orientation becomes more important to cause a great storm.

3. Comparison Between Theoretical Results and Observations

We have presented a clear modelled picture of flux rope's geoeffectiveness depending on its orientation. It implies a possible method to perform a long-term prediction of MC-caused geomagnetic storms without in situ observations at 1 AU if we could predict the parameters of MCs before their arrivals. However, in practice, magnetic clouds are not ideal flux ropes. They are usually deformed due to the interaction between MCs and ambient solar wind plasma, and therefore not necessarily cylindrically symmetric. For example, Mulligan and Russell (2001) and Mulligan *et al.* (2001) used two-spacecraft data to infer oblate cross sections, and Riley *et al.* (2003) showed that non-cylindrical MCs predicted from MHD simulations provide a better fit to a two-spacecraft data set than a simple cylindrical model. Thus the estimated intensity of MC-caused geomagnetic activity might be different from the observed values. This fact will undoubtedly reduce the application value of this method.

To assess the applicability of using an ideal flux rope model to predict real MC-caused geomagnetic storms, we investigate all the MC-associated moderate to large geomagnetic storms during 1998 – 2003, in which the Dst index from the World Data Center for Geomagnetism at Kyoto University and the interplanetary observations of solar wind plasma and magnetic field from the ACE spacecraft are used. The following criteria are applied to

Table 1 Magnetic clouds associated with moderate to large geomagnetic storms during 1998 – 2003.

No.	Date	Observations					Fitted parameters								Dst_{pe}[m]	Dst_{po}[n]
		T[a]	V[b]	n[c]	B[d]	B_s[d]	B_0[e]	H[f]	θ[g]	ϕ[h]	t_c[i]	R[j]	D[k]/R	χ^2/cc[l]		
1	1998.5.2 – 3	11.9 – 41.0	534	7.2	15	14	15.0	1	−57	346	22	27.6	0.316	0.063/0.92	−52	−85
2	1998.8.20 – 21	8.0–43.3	331	8.4	17	12	17.6	1	−4	307	19	16.3	−0.162	0.099/0.92	−21	−67
3	1998.8.27	7.2–18.2	597	3.5	17	15	12.5	−1	−33	336	5	9.1	0.121	0.071/0.98	−148	−155
4	1998.10.19	3.9–14.3	404	5.0	28	22	18.3	−1	−32	323	6	9.5	0.364	0.021/0.99	−85	−110
5	1998.11.9 – 10	4.1–25.5	442	9.2	18	16	17.5	1	−68	14	5	18.2	−0.029	0.051/0.95	−80	−142
6	1998.11.13 – 14	4.5–30.7	379	12.5	21	19	19.8	1	−86	178	15	18.5	−0.177	0.099/0.92	−54	−131
7	1999.4.16 – 17	22.1–43.0	408	13.4	25	15	24.1	−1	−15	129	31	10.1	−0.156	0.063/0.95	−33	−90
8	2000.7.15 – 16	19.7–35.7	850	1.6	55	54	45.5	−1	0.2	70	25	7.9	0.051	0.065/0.92	−289	−301
9	2000.8.10 – 11	19.3–42.1	424	3.0	14	14	11.5	−1	−44	3	18	19.2	−0.417	0.057/0.97	−25	−106
10	2000.8.12 – 13	5.2–25.0	580	9.0	34	30	35.9	−1	−33	115	13	11.5	0.174	0.069/0.94	−166	−235
11	2000.10.13 – 14	16.8–29.4	402	4.3	13	11	12.6	1	−52	47	22	13.4	0.329	0.020/0.99	−24	−107
12	2000.10.28 – 29	23.0–46.3	380	4.3	20	18	18.3	−1	−57	187	21	20.8	−0.168	0.017/0.99	−99	−127
13	2000.11.6 – 7	22.5–41.1	532	4.4	25	17	24.5	−1	−7	118	32	10.6	0.217	0.037/0.97	−151	−159
14	2001.3.19 – 21	23.4–70.2	360	6.3	22	21	26.0	−1	−72	286	29	20.5	0.459	0.032/0.96	−83	−149
15	2001.4.21 – 23	23.7–47.3	359	9.9	16	14	14.0	−1	−45	289	32	11.5	0.261	0.036/0.96	−4	−102
16	2002.3.24 – 25	11.9–38.0	437	5.3	20	13	18.9	1	37	314	31	20.1	−0.163	0.044/0.97	−79	−97
17	2002.4.18 – 19	1.0–25.9	478	1.8	15	14	12.0	1	−54	163	0	20.4	−0.181	0.069/0.93	−78	−127
18	2003.3.20	12.5–22.5	649	2.0	13	9	14.1	−1	−82	214	16	6.8	0.404	0.027/0.97	−37	−57
19	2003.10.29 – 30	11.4–26.1	1200	6.0	49	30	52.5	−1	−12	246	15	6.5	0.508	0.038/0.95	−399	−363
20	2003.11.20 – 21	10.1–24.4	589	13.4	56	53	50.0	1	−70	90	15	7.2	0.0	0.064/0.95	−327	−472

[a]Hours of the start and end of a magnetic cloud from the beginning of the date listed in the 2nd column.

[b]Average speed of a magnetic cloud (in km s^{-1}).

[c]Average number density of solar wind plasma within a magnetic cloud (in cm^{-3}).

[d]Maximum of magnetic field strength and the southward component of the magnetic field inside a magnetic cloud (in nT).

[e]Magnetic field magnitude at the axis of the flux rope (in nT).

[f]Sign of helicity of the flux rope, *i.e.*, handedness.

[g]Elevation angle of axial field (*i.e.*, axis) of the flux rope in GSE coordinates.

[h]Azimuthal angle of axial field (*i.e.*, axis) of the flux rope in GSE coordinates.

[i]Time at the closest approach to the axis of the flux rope.

[j]Radius of the flux rope (in hours).

[k]The signed closest distance between the axis of the flux rope and the x-axis in GSE coordinates (in hours). See text for more details.

[l]Goodness-of-fit. RMS deviation/correlation coefficient.

[m]Estimated minimum *Dst* value by applying the flux rope model and (1).

[n]Observed minimum *Dst* value from the World Data Center for Geomagnetism at Kyoto University.

selected events: (1) it was a storm with $Dst \leq -50$ nT; (2) it was mainly caused by an MC itself, but not something else, *e.g.*, the shock sheath ahead of the MC. MCs are identified based on the signatures first suggested by Burlaga *et al.* (1981). We expect that, for the events satisfying the two criteria, the MC's contribution to geomagnetic storms would be dominant, and the contamination by other factors should be efficiently reduced.

A total of twenty events are chosen as listed in Table 1. The third column gives the hours of the start and end of these MCs from the beginning of the date given in the second column. The fourth and fifth columns list the average solar wind speed and number density. The next two columns give the maximum values of the magnitude, B, and the southward component, B_s, of magnetic fields inside these MCs. The last column lists the observed minimum *Dst*

value, Dst_{po}. It should be mentioned that there were 14 storms with $Dst \leq -200$ nT from 1998 to 2003 but only 4 storms are selected due to the second criterion. Those unselected geomagnetic storms were mainly caused by the shock compressed region/shock sheath, MC-like structure or multiple-magnetic-cloud structure. Wang, Ye, and Wang (2003c) and Xue *et al.* (2005) have given the detailed analysis of some extremely large storms during 2000 – 2001.

The force-free flux rope model is used to fit the observed MCs as we did in our previous work (Wang, Wang, and Ye, 2002; Wang, Ye, and Wang, 2003c). A total of seven free parameters are fitted: (1) B_0, (2) $H = \pm 1$, (3) R_0, (4) θ, (5) ϕ, (6) D, and (7) t_c. The meaning of the first six parameters is the same as mentioned above, and the last one denotes the time when the spacecraft at the L1 point most closely approaches the MC axis. We make half-hourly data averages and apply a least-squares program (Marquardt, 1963) to fit the observations. The 8th through 14th columns give all the fitted parameters.

The goodness-of-fit is listed in the 15th column in which two indicators are given. One is RMS deviation (χ^2) calculated by the following formula

$$\chi^2 = \sum \left[\left(B_x - B_x^f\right)^2 + \left(B_y - B_y^f\right)^2 + \left(B_z - B_z^f\right)^2 \right] / N, \tag{2}$$

where the superscript 'f' indicates the fitting data of magnetic fields, N is the number of field vectors, and B and B^f are both unit normalized. The other indicator is correlation coefficient (cc). The goodness-of-fit of all these 20 MCs are high. Figure 5, for example, shows the fitting result of a well-known event on November 20, 2003. The fitting curves match the observations well. These results suggest that the ideal cylindrical flux rope is a reasonable approximation to these MCs.

Having obtained the parameters of the flux rope for each MC, we can predict the intensity of geomagnetic activity caused by the inferred flux rope, and compare it with the observed value. As described in Section 2, $B_z(t)$ required by the *Dst* calculator (1) can be inferred from the fitted parameters. The observed average solar wind speed and density are adopted as $V(t)$ and $n(t)$, respectively. Using constant V and n will not distort the result significantly, because the amplitudes of their fluctuations are generally much less than their average values. Besides, using constant V and n will make the long-term prediction more possible and easier.

A very important factor affecting the estimated *Dst* value is the initial *Dst* value. This effect can be seen clearly from (1). With different initial value, the estimated *Dst* value would be much different. For the comparability between the estimated and observed minimum *Dst* values, an initial *Dst* value should be taken into account. The interplanetary data of MCs are from the ACE spacecraft located at the L1 point. Therefore there is a significant delay time from the L1 point to the Earth. In terms of the solar wind speed and the distance from the L1 point to the magnetopause, the delay time can be deduced as ∼45 minutes in average. Considering this delay time and the time taken for the process of energy transfer from the solar wind to the ring current, we use the observed *Dst* value approximately one hour after the beginning of an MC as the initial *Dst* value.

The second to last column of Table 1 lists the estimated minimum *Dst* values, Dst_{pe}. As discussed at the beginning of this section, Dst_{pe} is not expected and does not closely match Dst_{po}. However, a correlation analysis reveals that there is a close linear correlation between the two data sets as shown in Figure 6. The linear correlation coefficient is about 0.930. The probability of such a correlation rising by chance between two random 20-element time series is as small as 2.9×10^{-9} which means a highly probable correlation. Although the errors between the estimated and observed minimum *Dst* values for some events are significantly

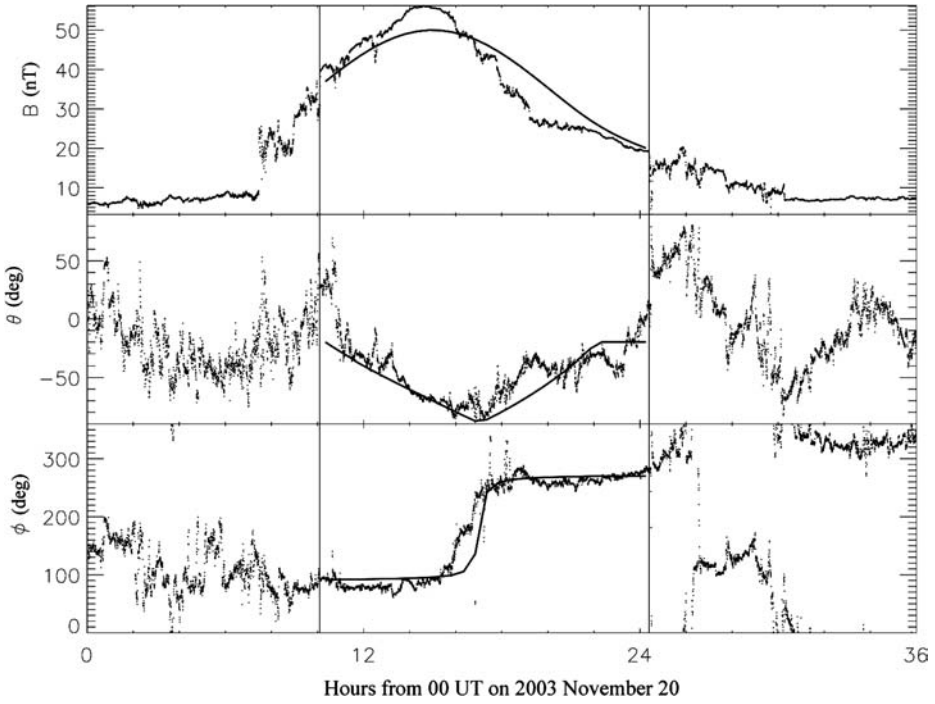

Figure 5 The observations of interplanetary magnetic field and fitting curves of 2003 November 20 magnetic cloud (in GSE coordinates).

large, the high correlation coefficient does imply that using inferred flux rope to estimate the intensity (at least relative intensity) of MC-caused geomagnetic storms is possible and applicable. This method will show its merits when we can predict the parameters of MCs before their arrivals.

4. Summary and Discussion

Based on the Lundquist (1950) force-free flux rope model and the Wang, Chao, and Lin (2003a) *Dst* model, the dependence of the intensity of geomagnetic activity on flux rope orientation has been studied theoretically. The distribution of estimated Dst_p in the (θ, ϕ) plane is calculated for a flux rope with various parameters. Some results are obtained: (i) Geomagnetic storms tend to occur for flux ropes with negative θ values, especially $\theta \lesssim -45°$, where large storms could be caused; (ii) The intensity of geomagnetic activity depends more strongly on θ than ϕ; (iii) When the parameter B_0, R_0, or V increases, or $|D|$ decreases, a flux rope not only can increase the intensity of geomagnetic activity, but also is more likely to create a storm, however the variation of n only has a little effect on the intensity; (iv) The most efficient orientation in which a flux rope can cause the largest geomagnetic activity appears at $\phi \sim 0°$ or $\sim 180°$ and a certain value of θ that depends primarily on D, marginally on B_0, R_0 and V, and negligibly on n; (v) The minimum Dst_p that could be caused by a flux rope is the most sensitive to changes in B_0 and V of the flux rope, and for a stronger and/or faster MC, a wider range of the MC orientation will be geoeffective.

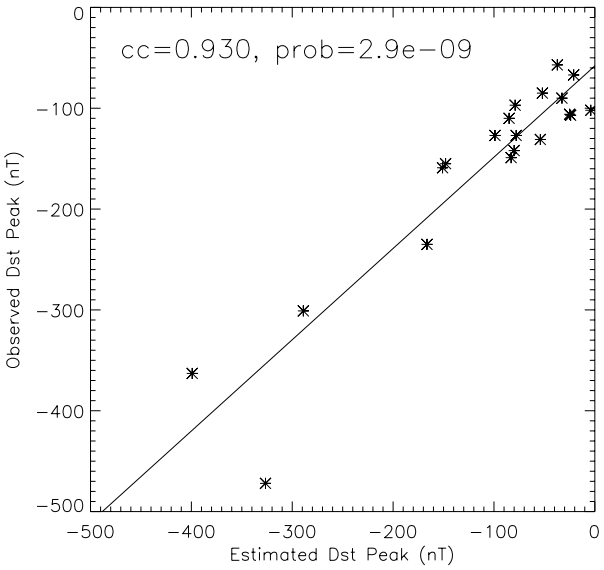

Figure 6 The correlation between the estimated and observed minimum *Dst* values.

It has been known for a long time that larger B_s and longer duration of B_s can produce more intense geomagnetic activity. However, in which orientation an MC has the best combination of B_s and its duration Δt that can cause the largest geomagnetic activity is not so apparent. Wang *et al.* (2003b) pointed out that the weights of B_s and Δt are different in causing geomagnetic storms. The former is much more important than the latter, especially for large geomagnetic storms. That is why the compressed interplanetary structures are more geoeffective as illustrated in the paper by Xue *et al.* (2005). Thus the MEO tends to be near the orientation with the largest B_s, which requires the MC to be highly inclined ($\theta \lesssim -45°$) as concluded in the last paragraph.

Further, the analysis of the 20 MC-caused moderate to large geomagnetic storms during 1998 – 2003 shows that, although the estimated minimum *Dst* values do not closely match the observed values, the estimated minimum *Dst* values do have a close linear correlation to the observed ones. This result implies that, at least, the relative intensity of MC-caused geomagnetic storms may be predicted, and if we could predict the parameters of MCs before their arrivals, a long-term prediction of MC-caused geomagnetic storms without *in situ* observations at 1 AU would be possible.

The hypothesized condition that we could predict the parameters of MCs before their arrivals is the base of our proposed long-term prediction, and at the present, it is not yet realized completely. However, a portion of this condition is likely to be resolved based on the current knowledge. Many case/statistical studies have shown that the magnetic field configurations of most MCs could be roughly inferred from the solar observations of the associated filaments, sigmoids or extending dimming (*e.g.*, Bothmer and Schwenn, 1994; Bothmer and Rust, 1997; Marubashi, 1997; McAllister *et al.*, 2001; Yurchyshyn *et al.*, 2001; Rust *et al.*, 2005; Fazakerley *et al.*, 2005). Certainly, only having the magnetic field configuration of MCs is not sufficient to make the long-term prediction of MC-caused geomagnetic storms. Other parameters, such as MC speed, density, size, *etc.*, are also required. Particularly, the MC speed and magnetic field strength strongly affect the capability of an MC in causing geomagnetic storms as shown in the lower panel of Figure 4. How to resolve these problems

is beyond the scope of this paper, but it is worthy to be attempted in the future. We believe that any efforts in this field would contribute to space weather prediction.

Acknowledgements We acknowledge the use of the interplanetary magnetic field and solar wind plasma data from the ACE spacecraft and the *Dst* index from the World Data Center for Geomagnetism at Kyoto University. We thank C.B. Wang for helpful discussion on the *Dst* model. We also express our thanks to Judy Karpen for partially improving the language of this paper. We thank the anonymous referee for improving the paper in both the scientific content and the language. This work is supported by the Grants from the NSF of China (40525014, 40404014, 40336052), the CAS (KZCX3-SW-144 and startup fund), the MOST of China (2006CB806304), and the Program for New Century Excellent Talents in University (NCET-04-0578).

References

Bothmer, V., Rust, D.M.: 1997, The field configuration of magnetic clouds and the solar cycle. In: Crooker, N., Joselyn, J.A., Feynman, J. (eds.) *Coronal Mass Ejections*, *Geophys. Monogr. Ser.* **99**, AGU, p. 139.

Bothmer, V., Schwenn, R.: 1994, Eruptive prominences as sources of magnetic clouds in the solar wind. *Space Sci. Rev.* **70**, 215.

Burlaga, L.F.: 1988, Magnetic clouds and force-free field with constant alpha. *J. Geophys. Res.* **93**, 7217.

Burlaga, L., Sittler, E., Mariani, F., Schwenn, R.: 1981, Magnetic loop behind an interplanetary shock: Voyager, Helios, and IMP 8 observations. *J. Geophys. Res.* **86**(A8), 6673.

Burton, R.K., McPherron, R.L., Russell, C.T.: 1975, An empirical relationship between interplanetary conditions and *Dst*. *J. Geophys. Res.* **80**, 4204.

Fazakerley, A.N., Harra, L.K., Culhane, J.L., van Driel-Gesztelyi, L., Lucek, E., Matthews, S.A., Owen, C.J., Mazelle, C., Balogh, A., Réme, H.: 2005, Relating near-Earth observations of an interplanetary coronal mass ejection to the conditions at its site of origin in the solar corona. *Geophys. Res. Lett.* **32**(13), L13105.

Fenrich, F.R., Luhmann, J.G.: 1998, Geomagnetic response to magnetic clouds of different polarity. *Geophys. Res. Lett.* **25**(15), 2999.

Gonzalez, W.D., Tsurutani, B.T.: 1987, Criteria of interplanetary parameters causing intense magnetic storms ($Dst < -100$ nT). *Planet. Space Sci.* **35**, 1101.

Gonzalez, W.D., Tsurutani, B.T., Gonzalez, A.L.C., Smith, E.J., Tang, F., Akasofu, S.I.: 1989, Solar wind – magnetosphere coupling during intense magnetic storms (1978 – 1979). *J. Geophys. Res.* **94**, 8835.

Gonzalez, W.D., Joselyn, J.A., Kamide, Y., Kroehl, H.W., Rostoker, G., Tsurutani, B.T., Vasyliunas, V.M.: 1994, What is a geomagnetic storm? *J. Geophys. Res.* **99**, 5771.

Gosling, J.T., McComas, D.J., Phillips, J.L., Bame, S.J.: 1991, Geomagnetic activity associated with earth passage of interplanetary shock disturbances and coronal mass ejections. *J. Geophys. Res.* **96**, 731.

Kumar, A., Rust, D.M.: 1996, Interplanetary magnetic clouds, helicity conservation, and current – core flux-ropes. *J. Geophys. Res.* **101**, 15667.

Lepping, R.P., Jones, J.A., Burlaga, L.F.: 1990, Magnetic field structure of interplanetary magnetic clouds at 1 AU. *J. Geophys. Res.* **95**, 11957.

Lundquist, S.: 1950, Magnetohydrostatic fields. *Ark. Fys.* **2**, 361.

Lundstedt, H., Gleisner, H., Wintoft, P.: 2002, Operational forecasts of the geomagnetic *dst* index. *Geophys. Res. Lett.* **29**(24), 2181, doi:10.1029/2002GL016151.

Marquardt, D.: 1963, An algorithm for least-squares estimation of nonlinear parameters. *J. Soc. Ind. Appl. Math.* **11**, 431.

Marubashi, K.: 1997, Interplanetary magnetic flux ropes and solar filaments. In: Crooker, N., Joselyn, J.A., Feynman, J. (eds.) *Coronal Mass Ejections*, *Geophys. Monogr. Ser.* **99**, AGU, p. 147.

McAllister, A.H., Martin, S.F., Crooker, N.U., Lepping, R.P., Fitzenreiter, R.J.: 2001, A test of real-time prediction of magnetic cloud topology and geomagnetic storm occurrence from solar signatures. *J. Geophys. Res.* **106**(A12), 29185.

Mulligan, T., Russell, C.T.: 2001, Multispacecraft modeling of the flux rope structure of interplanetary coronal mass ejections: Cylindrically symmetric versus nonsymmetric topologies. *J. Geophys. Res.* **106**(A6), 10581.

Mulligan, T., Russell, C.T., Anderson, B.J., Acuna, M.H.: 2001, Multiple spacecraft flux rope modeling of the Bastille Day magnetic cloud. *Geophys. Res. Lett.* **28**(23), 4417.

Murayama, T.: 1986, Coupling between solar wind and the *Dst* index. In: Kamide, Y., Slavin, J.A. (eds.) *Solar Wind – Magnetosphere Coupling*, Terra Scientific, Tokyo, p. 119.

O'Brien, T.P., McPherron, R.L.: 2000, Forecasting the ring current index *dst* in real time. *J. Atmos. Solar Terr. Phys.* **62**, 1295.

Perreault, P., Akasofu, S.-I.: 1978, A study of geomagnetic storms. *Geophys. J.* **54**, 547.
Riley, P., Linker, J.A., Mikic, Z., Odstrcil, D., Zurbuchen, T.H., Lario, R.P., Lepping, D.: 2003, Using an mhd simulation to interpret the global context of a coronal mass ejection observed by two spacecraft. *J. Geophys. Res.* **108**(A7), 1272, doi:10.1029/2002JA009760.
Rust, K., Anderson, B.J., Andrews, M.D., Acuna, M.H., Russell, C.T., Schuck, P.W., Mulligan, T.: 2005, Comparison of interplanetary disturbances at the NEAR spacecraft with coronal mass ejections at the SUN. *Astrophys. J.* **621**, 524.
Sheeley Jr., N.R., Howard, R.A., Koomen, M.J., Michels, D.J., Schwenn, R., Muhlhauser, K.H., Rosenbauer, H.: 1985, Coronal mass ejections and interplanetary shocks. *J. Geophys. Res.* **90**(A1), 163.
Temerin, M., Li, X.: 2002, A new model for the prediction of *dst* on the basis of the solar wind. *J. Geophys. Res.* **107**(A12), 1472, doi:10.1029/2001JA007532.
Tsurutani, B.T., Gonzalez, W.D.: 1995, The future of geomagnetic storm predictions: Implications from recent solar and interplanetary observations. *J. Atmos. Ter. Phys.* **57**, 1369.
Vasyliunas, V.M., Kan, J.R., Akasofu, S.-I., Siscoe, G.L.: 1982, Scaling relations governing magnetospheric energy transfer. *Planet. Space Sci.* **30**, 359.
Wang, C.B., Chao, J.K., Lin, C.-H.: 2003, Influence of the solar wind dynamic pressure on the decay and injection of the ring current. *J. Geophys. Res.* **108**(A9), 1341.
Wang, Y.M., Wang, S., Ye, P.Z.: 2002, Multiple magnetic clouds in interplanetary space. *Solar Phys.* **211**, 333.
Wang, Y.M., Ye, P.Z., Wang, S.: 2003, Multiple magnetic clouds: Several examples during March – April, 2001. *J. Geophys. Res.* **108**(A10), 1370, doi:10.1029/2003JA009850.
Wang, Y., Shen, C.L., Wang, S., Ye, P.Z.: 2003, An empirical formula relating the geomagnetic storm's intensity to the interplanetary parameters: $-\overline{VB_z}$ and Δt. *Geophys. Res. Lett.* **30**(20), 2039, doi:10.1029/2003GL017901.
Xue, X.H., Wang, Y., Ye, P.Z., Wang, S., Xiong, M.: 2005, Analysis on the interplanetary causes of the great magnetic storms in solar maximum (2000 – 2001). *Planet. Space Sci.* **53**, 443.
Yurchyshyn, V.B., Wang, H., Goode, P.R., Deng, Y.: 2001, Orientation of the magnetic fields in interplanetary flux ropes and solar filaments. *Astrophys. J.* **563**, 381.
Zhao, X.P.: 2002, The geoeffectiveness of frontside full halo coronal mass ejections. In: Wang, H., Xu, R. (eds.) *Proceedings of the COSPAR Colloquium held in the NAOC in Beijing, China*, *COSPAR Colloquia Series* **14**, 209.